Carotid dysfunction in senescent female mice is mediated by increased α_{1A}-adrenoceptor activity and COX-derived vasoconstrictor prostanoids.

Running title: carotid α-adrenergic dysfunction in female senescent mice

Tiago J. Costa[a,d], Paula R. Barros[a], Diego A. Duarte[a,b], Júlio A. Silva-Neto[a], Sara Cristina Hott[a], Thamyris Santos-Silva[a], Claudio M. Costa-Neto[b], Felipe V. Gomes[a], Eliana H. Akamine[c], Cameron G McCarthy[d], Francesc Jimenez-Altayó[e], Ana Paula Dantas*[f]. Rita C. Tostes*[a]

[a] Department of Pharmacology, Ribeirao Preto Medical School, University of São Paulo, Ribeirão Preto, SP, Brazil.
[b] Department of Biochemistry and Immunology, School of Medicine. campus Ribeirão Preto, University of São Paulo, Ribeirão Preto, SP, Brazil.
[c] Department of Pharmacology, Institute of Biomedical Sciences, University of São Paulo, São Paulo, SP, Brazil.
[d] Cardiovascular Translational Research Center, Department of Cell Biology and Anatomy, University of South Carolina, Columbia, South Carolina.
[e] Department of Pharmacology, Therapeutic. and Toxicology, School of Medicine, Neuroscience Institut, Universitat Autònoma de Barcelona, Bellaterra, Spain.
[f] Laboratory of Experimental Cardiology, Institut d'Investigacions Biomediques August Pi i Sunyer (IDIBAPS), Hospital Clinic Cardiovascular Institute, Barcelona, Spain.

*These authors jointly supervised this work

Corresponding Author:
Ana Paula Dantas - Laboratory of Experimental Cardiology, August Pi i Sunyer Biomedical Research Institute (IDIBAPS), Hospital Clinic Cardiovascular Institute, Barcelona, Spain. adantas@recerca.clinic.cat

Abstract

Alpha-adrenergic receptors are crucial regulators of vascular hemodynamics and essential pharmacological targets for cardiovascular diseases. With aging, there is an increase in sympathetic activation, which could contribute to the progression of aging-associated cardiovascular dysfunction, including stroke. Nevertheless, there is little information directly associating adrenergic receptor dysfunction in the blood vessels of aged females. This study determined the role of a-adrenergic receptors in carotid dysfunction of senescent female mice (accelerated-senescence prone, SAMP8), compared to a non-senescent (accelerated-senescence prone, SAMR1). Vasoconstriction to phenylephrine (Phe) were markedly increased in common carotid artery of SAMP8 (AUC: 527±53) compared to SAMR1 (AUC: 334±30, p= 0.006). There were no changes in vascular responses to the vasoconstrictor agent U46619 or the vasodilators acetylcholine (ACh) and sodium nitroprusside (NPS). Hyperactivity to Phe in female SAMP8 was reduced by cyclooxygenase-1 and cyclooxygenase-2 inhibition and associated with augmented ratio of TXA2/PGI2 release (SAMR1: 1.1±0.1 vs. SAMP8: 2.1±0.3, p= 0.007). However, no changes in cyclooxygenase expression were seen in SAMP8 carotids. Selective a1A receptor antagonism markedly reduced maximal contraction, while a1D antagonism induced a minor shift in Phe contraction in SAMP8 carotids. Ligand binding analysis revealed a 3-fold increase of α-adrenergic receptor density in smooth muscle cells (VSMC) of SAMP8 versus SAMR1. Phe rapidly increased intracellular calcium (iCa+2) in VSMC via the a1A receptor, with a higher peak in VSMC from SAMP8,. In conclusion, senescence intensifies vasoconstriction mediated by a1A-adrenergic signaling in the carotid of female mice by mechanisms involving increased iCa+2 and release of cyclooxygenase-derived prostanoids.

Key Words: Senescence, alpha-adrenergic receptor, cerebrovascular function, menopause, common carotid, senescence-accelerated mice

Introduction

Vascular dysfunction and the associated risk of Cardiovascular Diseases (CVD) increase with age in both men and women, although sex-associated differences exist regarding their incidence and severity of CVD. Cardiovascular diseases are less frequent in women at younger ages; however, they become more prevalent with aging (El Khoudary, Aggarwal et al. 2020). Since the elderly population is growing worldwide, elucidating the mechanisms of aging- and sex-associated vascular dysfunction is critical for better direct pharmacological and lifestyle interventions to prevent cardiovascular risk in both sexes.

In the central nervous system, vascular aging induces functional and structural alterations of the brain circulation, contributing to the pathogenesis of cognitive impairment, Alzheimer's disease, eye disease (e.g., glaucoma), and stroke (Niccoli and Partridge 2012). Epidemiological studies have suggested that women have worse outcomes in neurovascular disease than age-matched men. Strokes are more severe and show higher case fatality at one month among women (Appelros, Stegmayr et al. 2009). Moreover, women might have a higher burden of small vessel disease in the brain that could contribute to faster cognitive decline (Levine, Gross et al. 2021).

Classically, vascular dysfunction during aging is attributed to arterial stiffness or increased pulse wave velocity of large arteries (Ogola, Abshire et al. 2022), and endothelial dysfunction, in association with increased in reactive oxygen species (ROS) generation and quenching of nitric oxide (NO) bioavailability (Liguori, Russo et al. 2018). Moreover, an imbalance of COX-derived vasoconstrictor and vasodilator metabolites has also been implicated as an essential factor in the pathophysiology of vascular aging (Tang and Vanhoutte 2008). In addition to endothelial dysfunction, increased resting sympathetic nerve activity has also been described with aging and pointed out as a crucial factor in the pathophysiology of hypertension and heart failure in the elderly (Esler, Thompson et al. 1995, Balasubramanian, Hall et al. 2019). Sympathetic fibers innervate peripheral and cerebral vasculature, and sympathetic discharge is a crucial regulator of vasomotor tone and homeostasis in several tissues, including the brain (Willie, Tzeng et al. 2014). Nonetheless, there is little information on how aging changes sympathetic signaling in the cerebrovascular circulation, and even less is known about how this effect would influence female cerebrovascular health. Therefore, further investigation into how aging affects the mechanisms of sympathetic vasoconstriction in females is warranted.

To address our knowledge about the influence of aging on adrenergic signaling in the cerebral vasculature, we used the senescence-accelerated to study of vascular aging (Novella, Dantas et al. 2010, Novella, Dantas et al. 2013, Onetti, Jiménez-Altayó

et al. 2013) and age-associated cognitive diseases (Miyamoto 1997, Cosín-Tomás, Álvarez-López et al. 2018). This mouse model displays a spontaneous age-related deterioration of learning and memory compared to the control senescence-accelerated mouse resistant (SAMR1) strain (Butterfield and Poon 2005). In the vascular system, ovariectomized SAMP8 females present vascular morphological alterations and endothelial dysfunction (Novella, Dantas et al. 2010), and many of these abnormalities which are not improved by estrogen treatment (Costa, Jiménez-Altayó et al. 2019).

The brain vasculature consists of a dense network of arterioles that receive most of its supply from the carotid arteries system, which carry approximately 70% of the total cerebral blood flow (Willie, Tzeng et al. 2014). The cephalic circulation, mediated by the carotid artery, is an essential vascular bed to maintain adequate blood supply to the brain and prevent ischemia and tissue hypoxia. Therefore, the present study aims to determine the responses and mechanisms of α_1-adrenergic subtypes activation in the carotid artery of females in non-senescent (SAMR1) and senescent (SAMP8) mouse. In this study, we hypothesized that isolated carotid arteries from senescent SAMP8 females present augmented specific α_1-adrenergic responses compared to non-senescent SAMR1. SAMR1.

Material and Methods

Animal Models

Female senescence-accelerated mouse-prone 8 (SAMP8, n=42) and senescence-accelerated mouse resistant (SAMR1, n =42) were obtained from the breeding stock of the Pharmacology Department at the Biomedical Sciences Institute of the University of Sao Paulo (ICB-USP), and the *Parc Scientific* of Barcelona. Mice were maintained according to institutional guidelines (constant room temperature of 22°C, 12-hour light/dark cycles, 60% humidity, and standard mice chow and water *ad libitum)*. All the procedures used in this study were approved and performed following the guidelines of the Ethics Committee of the Ribeirao Preto Medical School, University of Sao Paulo (number 267/2018) and the Ethics Committee of the University of Barcelona (Comitè Ètic d'Experimentació Animal — CEEA protocols: 134/12 and 583/14), following the *Guide for the Care and Use of Laboratory Animals*, published by the National Institutes of Health (NIH Publication No. 85-23, Revised 1996). Mice were used at 6-9 months of age and during the estrus phase of physiological oestrous. The oestrous cycle was determined by cell characterization in the vaginal smear. After euthanasia, carotid arteries were isolated for functional analysis, and abdominal fat, gastrocnemius muscle, and uterus were harvested for phenotypic analysis.

Measurement of Sex Hormones

Blood was collected from the vena cava into heparin-containing tubes after isoflurane euthanasia (5%). Blood was centrifugated at 10,000 g for 30 minutes (min), and 4°C, and the supernatant was stored at –80°C until the experiments were performed. Plasma levels of estrogen (#10006315), progesterone (#582601), and testosterone (#582701) were determined by commercially available competitive ELISA assays (Cayman Europe) following the manufacturer's instructions.

Determination of Arterial Blood Pressure

The indirect tail-cuff method was used to measure systolic blood pressure. After an initial adaptation process (preheated at 40°C for 5 min), systolic blood pressure was recorded and calculated as the average of 3 consecutive measurements.

Novel Object Recognition (NOR) test

The NOR test determined cognitive function in SAMP8 (6 and 9 months of age) and SAMR1 (9 months) as described (Gomes and Grace 2017). Each animal was placed in the center of a circular arena (D60 cm x H60 cm) and allowed to explore it for 10 minutes for habituation. The next day, the NOR test was conducted in the same arena. Animals were subjected to 2 trials separated by 1 hour (h). During the first trial (acquisition trial, T1), mice were placed in the arena containing two identical objects for 5 minutes. For the second trial (retention trial, T2), one of the objects presented in T1 was replaced by an unknown (novel) object. Animals were then placed back in the arena for 5 minutes. Object exploration was defined as the animal facing the object at approximately 2 cm distance while watching, licking, sniffing, or touching it with the forepaws. Recognition memory was assessed using the discrimination index, corresponding to the difference between the time exploring the novel and the familiar object, corrected for the total time exploring both objects [discrimination index = (novel − familiar/ novel + familiar)].

Senescence Assay

Cellular senescence in mice vascular tissue was determined by β-galactosidase activity using a cellular senescence activity kit (Cell Biolabs, Inc #CBA231)), according to the manufacturer’s instructions. Briefly, pulverized aortic tissue from SAMR1 and SAMP8 was incubated with 100µL of extraction buffer for 5 min under gentle shaking. Equal amounts of protein lysate (50 µg) were used to quantify the β-galactosidase staining. β-Galactosidase Assay Reagent was added to

the samples for 30 minutes at 37° C. After this period, the reaction was stopped by adding 100 µl of β-Galactosidase Assay Stop Solution to each sample. The fluorescence was read at 360 nm excitation and 465 nm emission using a plate reader immediately after incubation in a FlexStation® fluorimeter coupled to the SoftMax® Pro software (Molecular Devices, Sunnyvale, CA, United States). Total protein was quantified by the Bradford method (Biorad), and 18 months old C57Bl/6 mice lung was used as a positive control.

Vascular Reactivity Studies

The common carotid arteries were dissected from anesthetized (Isoflurane – 4-5% induction; 1.5-2% maintenance) 8 months-old SAMP8 and SAMR1 mice and cleaned from perivascular fat tissue and vagal innervation in ice-cold physiological salt solution (PSS) [(in mM: NaCl 130; $NaHCO_3$ 14.9, KCl 4.7, KH_2PO_4 1.18, $MgSO_4$ 1.17; $CaCl_2.2H_2O$ 1.56, EDTA 0.026 and glucose 5.5]. Carotid segments of 2 mm length with and without an intact endothelium were mounted in isometric wire myograph chambers filled with PSS warmed to 37 °C and aerated with 95% O_2 and 5% CO_2. After a 30-minute equilibration period and basal tension normalization, the common carotid segments were exposed three times (10 minutes intervals) to the receptor-independent depolarizing agent KCl (60 mM) until the contraction reached a stable plateau (~15 min) as previously described (Costa, Jiménez-Altayó et al. 2019, Proudman, Pupo et al. 2020). Endothelial integrity was tested by administration of a single concentration of acetylcholine (10^{-6} M) after a contraction induced by phenylephrine (Phe, 10^{-6} M). Endothelium-intact arteries exhibited60-80% of maximal relaxation, while endothelium-denuded arteries displayed less than 5% of relaxation. After washout and return to a stable baseline, arterial segments were exposed to increasing concentrations of phenylephrine (10^{-9} - 10^{-5} M, Sigma Aldrich P6126) and U46619 (10^{-9} - 10^{-5} M, Tocris1923), as well as the vasodilator agents acetylcholine (ACh: 10^{-9}-10^{-5} M, Sigma Aldrich A6625) and sodium nitroprusside (SNP, 10^{-9} - 10^{-5} M). The contribution of the endothelium-derived factors to the vascular responses was determined by incubating carotid segments with one of the following inhibitors: (1) non-selective nitric oxide synthase (NOS) inhibitor Nω-nitro-L-arginine methyl ester (L-NAME; 10^{-4} M); (2) superoxide anion (O_2^-) scavenger (Tempol, 10^{-5} M); (3) non-selective COX inhibitor (Indomethacin, 10^{-6} M); (4) selective COX-1 inhibitor (SC560, 10^{-5} M); or (5) selective COX-2 inhibitor (NS398, 10^{-6} M). The contribution of specific alpha-adrenergic receptors to Phe-induced contraction was determined by treating arteries with an α_{-1A} adrenergic antagonist (5 methyl-urapidil 10^{-8} – 10^{-6} M) and an α_{-1D} adrenergic antagonist (BMY 7378 10^{-8} – 10^{-6} M). Treatments with inhibitors and antagonists were

done for 30 min before the Phe concentration-effect curve and the drugs were kept throughout the protocol.

Contractions to Phe and U46619 are shown as a percentage (%) of the contractile response induced by 60 mM KCl and relaxations to ACh, and SNP are expressed as the percentage (%) of contraction to U46619 (10^{-7} M ~50% Rmax). The area under the concentration-response curve (AUC), maximal response (Emax), and half maximal effective concentration (EC_{50}) were used to measure cumulative responses induced by agonists in the presence of vehicle or specific drugs/inhibitors.

Measurement of prostaglandin production by aortic rings

At the end of each protocol evaluating vascular reactivity to Phe, the Krebs medium was removed from the myograph chambers and left for 30 min at room temperature to allow the conversion of thromboxane A_2 (TXA_2) and prostacyclin (PGI_2) to their breakdown products: TXB_2 and 6-keto PGF-1α, respectively. Samples were then frozen at − 80°C. A commercial enzyme immunoassay kit determined levels of TXB_2, 6-keto PGF-1α, and $PGF_2α$ (Cayman Europe, TXA_2#10004023 and PGI_2 #501100) following the manufacturer's instructions.

α-adrenergic Receptor Binding Assay

As previously described (Proudman, Pupo et al. 2020), binding experiments were performed in VSMCs from aortas of 8-10 months old SAMR1 and SAMP8. An equal number of cells (80,000) were seeded per well in 6-well culture plates and incubated with cold binding buffer (25 mM Tris-HCl pH 7.4, with 5 mM $MgCl_2$, 0.1% BSA, and 100 µg/mL bacitracin). Cells were incubated with 0.5 nM 7-methoxy-^{3}H Prazosin (PerkinElmer) for approximately 16 h at 4ºC. Cells were then washed twice with cold wash buffer and lysed by adding lysis buffer (48% urea, 2% NONIDET P-40, 3 M acetic acid). Cell lysates were transferred to scintillation tubes, and after the addition of scintillation liquid (PerkinElmer) and vigorous mixing, the radioactivity was measured using the Tri-Carb 20100TR liquid scintillation counter (PerkinElmer). Non-specific binding was obtained by radioactivity measurement in cells treated with 100 µM Oxymetazoline. Total protein from lysates was quantified by the Bradford method (Biorad). Specific binding was determined by total biding subtracted from non-specific binding, which was calculated (GraphPad Software Inc, San Diego, CA, USA) to be expressed as fmol of α-adrenergic receptor/ mg of protein.

Ca^{2+} measurement in Vascular Smooth Muscle Cells.

VSMCs were isolated from the aortas of 8 months-old female SAMR1 and SAMP8. Cultures were maintained in Dulbecco's modified Eagle's medium (Gibco-BRL, USA) supplemented with 10% fetal bovine serum (FBS) (Invitrogen, USA). At the fourth passage, cells were plated in pretreated black-walled, clear-bottomed 96-well polystyrene plates (Corning, NY, United States) at a density of 40,000 cells/well in Dulbecco's Modified Eagle Medium (DMEM) with 20% FBS and incubated for 24 hours at 37°C in a 5% CO_2. Cytosolic-free calcium (Ca^{2+}) was measured using the cell-permeant Fluo-4 acetoxymethyl ester probe (Invitrogen, UK #14201). Following 24 h, the medium was replaced with ~430 µM Fluo-4 solution in DMEM and incubated in the dark for 45 min at 37°C. After washouts and a 15 min equilibration period, basal fluorescence was acquired at 494/506 nm excitation/emission using the FlexStation® fluorimeter coupled to SoftMax® Pro software (Molecular Devices, Sunnyvale, CA, United States). After this period, the VSMCs were stimulated with phenylephrine 10^{-7} M, and the fluorescence was analyzed for 160 seconds. Ionomycin calcium salt (Tocris, #1704) was used as a positive control. Inhibition of adrenergic receptor α1a was performed in the presence of monoclonal rabbit IgG anti-α_{1a} antibody (Abcam #ab137123). A non-specific IgG antibody was used as a negative control in this set of experiments.

Quantitative real-time PCR (qPCR)

mRNA expression of the subtypes of alpha-adrenergic receptors ADRA1A (OMIM: 104221) and ADRA1D (OMIM: 104219) were quantified by Sybr green-based quantitative real-time (q)PCR, as previously described (Jiménez-Altayó, Onetti et al. 2013). The mouse-specific primer sequences were:

COX1 (NM_008969.3) Forward: 5'-GAGCCGTGAGATGGGTGGGAGGG-3', Reverse: 5'-TGGATGTGCAATGCCAACGGCT-3'; and COX2 (NM_011198.3) Forward: 5'-GTCAGGACTCTGCTCACGAAGGAAC-3', Reverse: 5'-ACAGCTCGGAAGAGCATCGCAG-3'. qPCR reactions were set following the manufacturer's conditions (Applied Biosystems-Thermo Fisher). Ct values obtained for each gene were normalized to Ct of housekeeping gene ACTB (ΔCt) and converted to the linear form using the term $2^{-\Delta Ct}$. Data were expressed as $2^{-\Delta\Delta Ct}$ relative to the average of SAMR1 expression.

Statistical analysis

Data are expressed as mean ± SEM. For analysis of vascular reactivity, individual concentration-effect curves were plotted on a sigmoidal curve by non-linear regression analysis. The extra sum-of-squares F determined the differences in the fit of concentration-response curves in all groups. The area under the curve (AUC) and pD_2

(negative logarithm of the EC_{50} values - concentration that produces 50% of the maximum response) were calculated for individual contractile or relaxing concentration-response curves and expressed as arbitrary units. The contribution of different endothelium-derived factors to Phe-induced contractions was calculated by subtracting the AUC for Phe curves in the presence of inhibitors from the AUC for control Phe curves (ΔChange). Brown Forsythe and Welch ANOVA compared means across three (or more) independent variables, followed by Dunnett's T3 posthoc analysis for multiple comparisons. The comparison of means across SAMR1 *vs.* SAMP8 and Basal *vs.* treatments was performed by unpaired T-test with Welch's correction. In the cognitive test (NOR), all the data were subjected to tests to verify the homogeneity of variances (Bartlett's test) and if they followed a normal distribution (Shapiro–Wilk test). Those that met these parameters were subjected to parametric analysis (One-Way ANOVA followed by Tukey's post-test). The statistical analysis was carried out using the Prism 9 software (GraphPad Software Inc., San Diego, CA, USA), and statistical significance was accepted at $p < 0.05$.

Results

Basic Parameters analyses

Senescent SAMP8 display a distinct metabolic profile, with increased abdominal obesity, decreased lean mass and increased body weight in comparison to SAMR1 **(Table 1, Supplementary Figure S1)**. The groups had similar levels of estrogen, testosterone, and progesterone **(Table 1)**. Interestingly, despite showing similar hormone levels, the uterine weight was decreased in SAMP8 compared to SAMR1, and female SAMP8 spent less time in estrus than SAMR1 **(Table 1, Supplementary Figure S1)**. There were no differences in blood pressure levels between SAMR1 and SAMP8 **(Table 1)**.

Cognitive function was determined by the NOR test **(Supplementary Figure S2A)**. During the habituation session, there were no differences in locomotor activity between the groups **(Supplementary Figure S2B)**. Although there was no difference between the exploration of the familiar objects placed on the right or left side of the arena during the training trial, SAMP8 (both at 6 and 9 months of age) spent more time exploring the objects than SAMR1 **(Supplementary Figure S2C)**, indicating a lack of spatial preference. In the retention trial, a greater exploration of the novel object was observed in 9 months-old (9M) SAMR1 (t_{22}= 4.260, $p<0.0003$) and 6 months-old (6M) SAMP8 (t_{22}= 4.830, $p<0.0002$), but not in 9M SAMP8 (t_{22}= 1.264, $p>0.05$) **(Supplementary Figure S2D)**. These findings were reflected in the discrimination

index **(Supplementary Figure S2E)**, showing a lower cognitive function in SAMP8 at 9 months compared to younger SAMP8 (6 months) and its respective non-senescent control SAMR1 at 9 months. In addition to cognition, the arteries of 8 months-old SAMP8, early state of lower cognition, presented signs of senescence in arteries as determined by increased β-galactosidase activity compared to SAMR1 **(Supplementary Figure S3) (Supplementary Figure S3)**, and for the next sets of experiments, SAMP8 and SAMR1 were tested at 8-months of age.

Vascular reactivity in the carotid artery

In carotid arteries of 8 months-old female SAMP8, the contractile responses to Phe were markedly increased compared to age-matched SAMR1, as demonstrated by the greater AUC and maximal contraction in vessels with **(Figure 1A, Supplementary Table S1)** or without endothelium **(Supplementary Figure S4, Supplementary Table S1)**. On the other hand, there were no differences in the contractile responses to U46619 **(Figure 1C)** or in the vasodilation to ACh **(Figure 1D)** and SNP **(Figure 1E)** in the common carotid rings of the SAMR1 and SAMP8 groups.

Next, we sought to elucidate the mechanisms involved in the Phe hypersensitivity found in the common carotid artery of SAMP8. We analyzed the contribution of the main endothelium-derived factors to the contractile response to Phe. Non-selective inhibition of NO production with L-NAME increased the vasoconstrictor responses to Phe in carotids of both SAMR1 **(Figure 2A)** and SAMP8 **(Figure 2B)**. In addition, scavenging of superoxide anion (O_2^-) with tempol decreased Phe contractions in common carotids from SAMP8 **(Figure 2D),** but did not affect the contractions in the carotid of SAMR1 **(Figure 2C)**. Carotid arteries were initially treated with the non-specific inhibitor of cyclooxygenases (COX) indomethacin, to determine the contribution of COX-derived prostanoids to the regulation of Phe-induced contractions in SAMP8. Indomethacin decreased Phe contraction in carotid arteries of SAMP8 **(Figure 2F)**, but not in SAMR1 arteries **(Figure 2E)**. The relative contribution of each endothelium-derived factor (NO, O_2^- or prostanoids) was analyzed by calculating the Δ Change in the AUC **(Figure 2G)**. This analysis showed an equal contribution of NO to the contractile responses to Phe in the arteries of SAMR1 and SAMP8. However, Δ Change in the AUC after COX inhibition was significantly increased in the SAMP8 group, suggesting a contribution of COX-derived vasoconstrictor metabolites to the vascular hyperreactivity to Phe in female SAMP8. No differences in the Δ Change in the AUC after tempol treatment were observed between the groups **(Figure 2G)**.

The specific role of COX isoenzymes in Phe contractions was then determined by incubating SAMR1 and SAMP8 carotids with the selective inhibitors of COX-1

(SC560) and COX-2 (NS398). Following the indomethacin response pattern, selective COX-1 and COX-2 inhibition did not modify Phe-induced contractions in vessels of SAMR1 **(Figure 3A; Figure 3B)**. On the other hand, in SAMP8, the inhibition of COX-1 and COX-2 decreased Phe-induced vasoconstriction **(Figure 3C; Figure 3D)**, suggesting increased production of COX-derived vasoconstrictor prostanoids in the carotid arteries of senescent mice. Prostanoid release from the common carotid artery was determined in the Krebs solution collected after concentration-response curves to Phe. In carotids from SAMP8, the release of PGI_2 was decreased by ~2-fold compared to SAMR1 arteries **(Figure 3E)**. Although the release of TXA_2 by Phe was similar between the groups **(Figure 3F),** the TXA_2/PGI_2 ratio was two times higher in SAMP8 than in SAMR1 **(Figure 3G)**, which could favor the more pronounced vasoconstriction in SAMP8 carotid arteries. Despite the differences in COX pathway activation, there were no changes in the expression of COX-1 **(Figure 3H)** or COX-2 **(Figure 3I)** in the common carotid of SAMP8 versus SAMR1.

Role of α_1 adrenergic receptor in the vascular hyperreactivity to Phe in SAMP8

In another set of experiments, carotids were treated with selective antagonists of α_{1A} (5methyl-urapidl) and α_{1D} (BMY7378) receptors to determine the role of the alpha adrenoceptors' subtypes in the vascular hyperreactivity to Phe in SAMP8. Different concentrations of both antagonists were tested in the common carotid of SAMR1 to establish the antagonist concentration used in the studies **(Figure 4A, Figure 4B)**. In arteries of SAMR1, the addition of 10^{-7} M of the α_{1A} **(Figure 4C)** or α_{1D} **(Figure 4D)** antagonists right-shifted the concentration-dependent curves to Phe**,** showing that both receptors contribute to Phe-induced contraction. However, in the carotid of SAMP8, α_{1A} antagonism blunted the maximal contraction to Phe **(Figure 4E)**, while α_{1D} antagonism induced a minor shift in Phe contraction **(Figure 4F)**. The density of α_1-adrenergic receptor was analyzed in primary VSMC cultures of female SAMR1 and SAMP8 . A single concentration of [^{3}H]-Prazosin was used to generate association binding in the absence [total biding] or in the presence of 100 μM Oxymetazoline [for non-specific biding] **(Figure 4G)**. Following normalization of [^{3}H]-Prazosin counts [cpm] with the amount of protein in each sample, we observed a marked increase in the affinity of α_1-adrenoreceptor in VSMC of SAMP8 **(Figure 4H)**, suggesting a higher density of the receptor.

Continuing the studies of α_1-adrenoreceptor activity in VSMC of SAMR1 and SAMP8, we determined changes in intracellular Ca^{+2} (iCa^{+2}) following activation of α_1 receptor with 10^{-7} M Phe **(Figure 5A)**. Although Phe induced a rapid increase of iCa^{+2}

393 in both groups, the peak of iCa^{+2} was significantly higher in VSMC from SAMP8 than in
394 SAMR1 VSMC **(Figure 5B, Figure 5E)**. Blockade of the α1a receptor with a
395 monoclonal antibody augmented Phe-induced iCa^{+2} in VSMCs from SAMR1 **(Figure**
396 **5C, Figure 5E),** while it decreased iCa^{+2} in cells from SAMP8 **(Figure 5D, Figure 5E).**
397
398 **Discussion**
399 This study shows that the conductance artery carotid from senescence females
400 present higher levels of adrenergic receptors and hyperactivity in response to alpha-
401 adrenergic receptor stimulation. At the beginning of senescence in the female SAMP8
402 model [as established in our previous studies (Novella, Dantas et al. 2010)], there are
403 increased constrictor responses to Phe in the carotid arteries mediated by α_{1A}-
404 adrenoceptor that in turn increase Ca^{+2} influx. In addition, this study observed changes
405 in prostanoid unbalance under Phe stimulus in the carotid of SAMP8 than SAMR1, that
406 impact Phe-induced vasoconstriction. To the best of our knowledge, no study has
407 described the specific alpha adrenergic subtype mechanisms in the carotid arteries of
408 senescent females at the functional and molecular levels. So far, only a few functional
409 studies on aging-associated sympathetic hyperactivity have focused on the carotid
410 vascular bed(de Oliveira, Campos-Mello et al. 1998, Omar, Abbas et al. 2013, Credeur,
411 Holwerda et al. 2014).
412 Senescence, *per se,* is known to cause a series of alterations in the
413 endogenous mechanisms that control cellular function leading to a subsequent
414 increase in organ dysfunction and the risk of cardiovascular disease. A correlation
415 between senescence and vascular dysfunction has been extensively described in men
416 and women and has been primarily associated with decreased NO-mediated
417 vasodilation (Sverdlov, Ngo et al. 2014) and platelets-derived NO (Goubareva,
418 Gkaliagkousi et al. 2007). However, as reviewed by Barros et al. 2021, the
419 physiological mechanisms that control vascular function during senescence differ in
420 males and females (Barros PR 2021).
421 The female senescence-accelerated mouse prone is an experimental model
422 that exhibits characteristics of senescence-associated dysfunction, including cognitive
423 (Miyamoto 1997) and vascular alterations (Novella, Dantas et al. 2013). In addition,
424 reproductive senescence in this model is associated with ovarian decline characterized
425 by periods of constant estrus cycle and lack of ovulation (Felicio, Nelson et al. 1984).
426 Despite not exhibiting changes in sex hormone levels, female SAMP8 spend more
427 time in diestrus than estrus (Novella, Dantas et al. 2013) at younger ages (Han,
428 Hosokawa et al. 1998) in comparison to SAMR1. In association with estrus cycle
429 dysregulation, we observed a reduction in uterine weight, increased abdominal fat, and

decreased gastrocnemius mass in SAMP8 compared to SAMR1 mice. These characteristics are similar to those seen in post-menopause women (Takahashi and Johnson 2015).

In this study, we found that vasoconstriction induced by the α-adrenergic agent Phe was the only response modified in the carotid arteries of SAMP8 at 8 months. There were no differences in the contractile responses to U46619 or vasodilation to ACh or NPS in the carotids of SAMP8 compared to SAMR1. In previous studies, we observed changes in vascular reactivity to the vasoconstrictor agent U46619 and to the endothelium-dependent vasodilator ACh in the aorta of female SAMP8 (Novella, Dantas et al. 2010, Novella, Dantas et al. 2013, Onetti, Jiménez-Altayó et al. 2013), suggesting a different mechanism in carotid and aorta dysfunction.

Differences in functional responses among the vascular beds may be related to their diverse origin and structures. In preliminary studies in female SAMP8, vascular reactivity in the descending thoracic aorta (developed from the somites). In contrast, in the present study, vasoactive responses were determined in the common carotid arteries that are branches of the brachiocephalic artery deriving from ascending aortic arch (whose origin is in the neural crest (Majesky 2007)]. A detailed study on the structural, genetic, and functional heterogeneity of VSMCs of a unique aorta demonstrated that cells from different embryonic origins are functionally distinct (Pfaltzgraff, Shelton et al. 2014). Therefore, the existence of a fingerprint of vascular function and dysfunction in each vascular bed is recognized, which must depend on the origin and environment in which the vessel is surrounded.

Different intrinsic mechanisms have been described to contribute to altered vascular responses in senescent vessels. The aorta of female SAMP8 presented an earlier, faster, and time-dependent decrease in NO and increased oxidants levels compared to SAMR1 (Novella, Dantas et al. 2010, Novella, Dantas et al. 2013, Onetti, Jiménez-Altayó et al. 2013), which may contribute to the observed aortic dysfunction. Yet, unlike other models of senescence or vascular beds in the same model, COX-derived metabolites were the only endothelium-derived factors modified in SAMP8 carotid arteries. Changes in Phe-induced contractions in female SAMP8 were associated with an increased ratio of the release of vasoconstrictors over vasodilator prostanoids. The higher TXA_2/PGI_2 ratio after Phe stimulation in the carotids of SAMP8 may favor the greater vasoconstriction observed. However, granting that the imbalance in prostanoid biosynthesis justifies the existence of vascular dysfunction in carotid arteries of SAMP8, this result does not explain why this dysfunction is unique to Phe responses, as there is no difference in the responses to other vasoactive agents, such as the vasoconstrictor U46619, a TXA_2 analog, or the endothelium-dependent

vasodilator ACh. A possible contribution of alternative pathways, such as the EDHF, could also provide a transitory compensatory response in the common carotid at this age-range. This hypothesis has not, however, been tested by us or other groups to date.

Chronic overactivity of the sympathetic nervous system is a hallmark of aging and contributes to developing several aging-associated diseases, including cardiovascular diseases (Balasubramanian, Hall et al. 2019). Over the last few decades, the neuronal mechanisms contributing to sympathetic overactivity were studied in detail only with limited success under pathophysiological conditions. Moreover, most studies present a more neurological than vascular approach (Balasubramanian, Hall et al. 2019).

The α-adrenergic signaling pathway is one of the central regulators of cerebrovascular tone and cerebral blood flow, and α-adrenergic vascular responses change with age, although not equally in the different vascular territories within the brain vasculature(Frost, Keable et al. 2020). In our study, we showed that vascular dysfunction of carotid arteries at early stages of senescence in female SAMP8 is associated with hyperactivity in response to adrenergic signaling in the vascular smooth muscle, rather than only endothelial dysfunction (Novella, Dantas et al. 2013). Increased Phe-induced contraction was observed in endothelium-intact and endothelium-denuded carotid arteries. We also observed a marked increase in binding affinity to α_1-adrenoreceptor that was paralleled by α_{1A}-mediated increased Ca^{2+} influx in vascular smooth muscle cells isolated from SAMP8. Our results and a few other studies in this field show that sympathetic regulation of cerebral circulation during aging is not a direct and uniform process and may vary depending on the vascular bed and pathophysiological conditions.

With aging, cognitive impairment results from nonvascular processes and vascular dysfunction (Kara, Gordon et al. 2023). In the present study, we observed that the onset of carotid vascular dysfunction is associated with impairments in cognitive function, reflected by the lower discrimination index observed in senescent females (9-months-old SAMP8) in the NOR test. Most studies on the vascular mechanisms of cognitive impairment are related to small vessel diseases that manifest as dysregulated neurovascular coupling and blood-brain barrier dysfunction (Fouda, Fagan et al. 2019, Kara, Gordon et al. 2023). Nonetheless, we cannot minimize the role of conductance arteries in microvascular dysfunction. Studies have suggested that carotid artery dysfunction, such as stenosis, is an independent risk factor for cognitive impairment and cardiovascular disease (Pettigrew, Thomas et al. 2000, Dutra 2012, Zhong, Cruickshanks et al. 2012, Heller and Hines 2017, Wang, Liu et al. 2017).

Although the carotid arteries do not have direct contact with the brain, they are essential suppliers of blood to the brain via the circle of Willis and key controllers of cerebral blood flow (for review (Dutra 2012). Moreover, it is well-established that changes in vascular contractility and elasticity of conductance vessels (including carotid arteries) modify the pattern of flow and pulsatility towards smaller vessels, modifying their vascular tone. In a prospective and community-based study, Mitchell et al. 2011 (Mitchell, van Buchem et al. 2011) described that reduced wave reflection at the interface between the carotid and aorta leads to the transmission of excessive flow pulsatility into the brain, microvascular structural brain damage and lower scores in various cognitive domains. In addition, this study showed that changes in carotid pulse pressure were associated with lower memory scores in this population. In the present study, despite the parallelism of the alpha-adrenergic hyperactivity in the common carotid with cognitive decline in senescent female mice, we are aware that our results do not directly test the contribution of changes in carotid adrenergic reactivity to cognition decline. Nonetheless, this study provides new insights into potential mechanisms for vascular-associated cognitive impairment during aging.

Conclusion

The present study provides evidence of increased α_{1A}-adrenoceptor signaling, linked to a functional impairment of common carotid of the female murine model of senescence (SAMP8). Increased alpha adrenergic reactivity of the common carotid artery during senescence is paralleled with cognitive decline in senescent females and may represent a potential mechanism for cognitive dysfunction with aging. Although our results do not provide direct evidence to associated carotid dysfunction with cognitive impairment, it furnishes the rational for the design of further experiments to determine the mechanisms of vascular senescence in cerebral dysfunction.

Acknowledgments

The authors thank Carla P. Manzato for excellent technical assistance and Prof Dr. Andre Sampaio Pulpo for an excellent discussion and suggestions in the analysis of alpha-adrenergic receptors and the binding technique. The graphical abstract was created using a licensed version of BioRender.

Source of Funding

This study was supported by The São Paulo State Research Foundation (FAPESP; Grant 2013/08216–2 to the Center of Research in Inflammatory Diseases), Conselho Nacional de Desenvolvimento Científico e Tecnológico (CNPq), Coordenação de

Aperfeiçoamento de Pessoal de Nível Superior (CAPES), Spanish funds from Ministerio de Economía y Competitividad, Instituto de Salud Carlos III - FEDER-ERDF (PI16/00742, PI19/00264). Tiago J. Costa is a FAPESP post-doctoral fellow (2017/25116–2 and 2019/26376–0).

Disclosures

The authors declare no competing interests.

References

Appelros, P., B. Stegmayr and A. Terént (2009). "Sex differences in stroke epidemiology: a systematic review." Stroke **40**(4): 1082-1090.

Balasubramanian, P., D. Hall and M. Subramanian (2019). "Sympathetic nervous system as a target for aging and obesity-related cardiovascular diseases." Geroscience **41**(1): 13-24.

Barros PR, C. T., Akamine EH, Tostes RC. (2021). Vascular Aging in Rodent Models: Contrasting Mechanisms Driving the Female and Male Vascular Senescence, Front. Aging.

Butterfield, D. A. and H. F. Poon (2005). "The senescence-accelerated prone mouse (SAMP8): a model of age-related cognitive decline with relevance to alterations of the gene expression and protein abnormalities in Alzheimer's disease." Exp Gerontol **40**(10): 774-783.

Cosín-Tomás, M., M. J. Álvarez-López, J. Companys-Alemany, P. Kaliman, C. González-Castillo, D. Ortuño-Sahagún, M. Pallàs and C. Griñán-Ferré (2018). "Temporal Integrative Analysis of mRNA and microRNAs Expression Profiles and Epigenetic Alterations in Female SAMP8, a Model of Age-Related Cognitive Decline." Front Genet **9**: 596.

Costa, T. J., F. Jiménez-Altayó, C. Echem, E. H. Akamine, R. Tostes, E. Vila, A. P. Dantas and M. H. C. Carvalho (2019). "Late Onset of Estrogen Therapy Impairs Carotid Function of Senescent Females in Association with Altered Prostanoid Balance and Upregulation of the Variant ERα36." Cells **8**(10).

Costa TJ, Barros PR, Arce C, Santos JD, da Silva-Neto J, Egea G, Dantas AP, Tostes RC, Jiménez-Altayó F (2021). The homeostatic role of hydrogen peroxide, superoxide anion and nitric oxide in the vasculature. Free Radic Biol Med.**162**:615-635

Credeur, D. P., S. W. Holwerda, L. J. Boyle, L. C. Vianna, A. K. Jensen and P. J. Fadel (2014). "Effect of aging on carotid baroreflex control of blood pressure and leg vascular conductance in women." Am J Physiol Heart Circ Physiol **306**(10): H1417-1425.

de Oliveira, A. M., C. Campos-Mello, M. C. Leitão and F. M. Correa (1998). "Maturation and aging-related differences in responsiveness of rat aorta and carotid arteries to alpha1-adrenoceptor stimulation." Pharmacology **57**(6): 305-313.

Dutra, A. P. (2012). "Cognitive function and carotid stenosis: Review of the literature." Dement Neuropsychol **6**(3): 127-130.

El Khoudary, S. R., B. Aggarwal, T. M. Beckie, H. N. Hodis, A. E. Johnson, R. D. Langer, M. C. Limacher, J. E. Manson, M. L. Stefanick, M. A. Allison, A. H. A. P. S. C. o. t. C. o. E. a. Prevention and a. C. o. C. a. S. Nursing (2020). "Menopause Transition and Cardiovascular Disease Risk: Implications for Timing of Early Prevention: A

586 Scientific Statement From the American Heart Association." Circulation:
587 CIR0000000000000912.
588 Esler, M. D., J. M. Thompson, D. M. Kaye, A. G. Turner, G. L. Jennings, H. S. Cox, G.
589 W. Lambert and D. R. Seals (1995). "Effects of aging on the responsiveness of the
590 human cardiac sympathetic nerves to stressors." Circulation **91**(2): 351-358.
591 Felicio, L. S., J. F. Nelson and C. E. Finch (1984). "Longitudinal studies of estrous
592 cyclicity in aging C57BL/6J mice: II. Cessation of cyclicity and the duration of persistent
593 vaginal cornification." Biol Reprod **31**(3): 446-453.
594 Fouda, A. Y., S. C. Fagan and A. Ergul (2019). "Brain Vasculature and Cognition."
595 Arterioscler Thromb Vasc Biol **39**(4): 593-602.
596 Frost, M., A. Keable, D. Baseley, A. Sealy, D. Andreea Zbarcea, M. Gatherer, H. M.
597 Yuen, M. M. Sharp, R. O. Weller, J. Attems, C. Smith, P. R. Chiarot and R. O. Carare
598 (2020). "Vascular α1A Adrenergic Receptors as a Potential Therapeutic Target for
599 IPAD in Alzheimer's Disease." Pharmaceuticals (Basel) **13**(9).
600 Gomes, F. V. and A. A. Grace (2017). "Prefrontal Cortex Dysfunction Increases
601 Susceptibility to Schizophrenia-Like Changes Induced by Adolescent Stress
602 Exposure." Schizophr Bull **43**(3): 592-600.
603 Goubareva, I., E. Gkaliagkousi, A. Shah, L. Queen, J. Ritter and A. Ferro (2007). "Age
604 decreases nitric oxide synthesis and responsiveness in human platelets and increases
605 formation of monocyte-platelet aggregates." Cardiovasc Res **75**(4): 793-802.
606 Han, J., M. Hosokawa, M. Umezawa, H. Yagi, T. Matsushita, K. Higuchi and T. Takeda
607 (1998). "Age-related changes in blood pressure in the senescence-accelerated mouse
608 (SAM): aged SAMP1 mice manifest hypertensive vascular disease." Lab Anim Sci
609 **48**(3): 256-263.
610 Heller, S. and G. Hines (2017). "Carotid Stenosis and Impaired Cognition: The Effect of
611 Intervention." Cardiol Rev **25**(5): 211-214.
612 Jiménez-Altayó, F., Y. Onetti, M. Heras, A. P. Dantas and E. Vila (2013). "Western-
613 style diet modulates contractile responses to phenylephrine differently in mesenteric
614 arteries from senescence-accelerated prone (SAMP8) and resistant (SAMR1) mice."
615 Age (Dordr) **35**(4): 1219-1234.
616 Kara, B., M. N. Gordon, M. Gifani, A. M. Dorrance and S. E. Counts (2023). "Vascular
617 and Nonvascular Mechanisms of Cognitive Impairment and Dementia." Clin Geriatr
618 Med **39**(1): 109-122.
619 Levine, D. A., A. L. Gross, E. M. Briceño, N. Tilton, B. J. Giordani, J. B. Sussman, R. A.
620 Hayward, J. F. Burke, S. Hingtgen, M. S. V. Elkind, J. J. Manly, R. F. Gottesman, D. J.
621 Gaskin, S. Sidney, R. L. Sacco, S. E. Tom, C. B. Wright, K. Yaffe and A. T. Galecki

(2021). "Sex Differences in Cognitive Decline Among US Adults." JAMA Netw Open **4**(2): e210169.
Liguori, I., G. Russo, F. Curcio, G. Bulli, L. Aran, D. Della-Morte, G. Gargiulo, G. Testa, F. Cacciatore, D. Bonaduce and P. Abete (2018). "Oxidative stress, aging, and diseases." Clin Interv Aging **13**: 757-772.
Majesky, M. W. (2007). "Developmental basis of vascular smooth muscle diversity." Arterioscler Thromb Vasc Biol **27**(6): 1248-1258.
Mitchell, G. F., M. A. van Buchem, S. Sigurdsson, J. D. Gotal, M. K. Jonsdottir, Ó. Kjartansson, M. Garcia, T. Aspelund, T. B. Harris, V. Gudnason and L. J. Launer (2011). "Arterial stiffness, pressure and flow pulsatility and brain structure and function: the Age, Gene/Environment Susceptibility--Reykjavik study." Brain **134**(Pt 11): 3398-3407.
Miyamoto, M. (1997). "Characteristics of age-related behavioral changes in senescence-accelerated mouse SAMP8 and SAMP10." Exp Gerontol **32**(1-2): 139-148.
Niccoli, T. and L. Partridge (2012). "Ageing as a risk factor for disease." Curr Biol **22**(17): R741-752.
Novella, S., A. P. Dantas, G. Segarra, L. Novensà, C. Bueno, M. Heras, C. Hermenegildo and P. Medina (2010). "Gathering of aging and estrogen withdrawal in vascular dysfunction of senescent accelerated mice." Exp Gerontol **45**(11): 868-874.
Novella, S., A. P. Dantas, G. Segarra, L. Novensa, M. Heras, C. Hermenegildo and P. Medina (2013). "Aging enhances contraction to thromboxane A2 in aorta from female senescence-accelerated mice." Age (Dordr) **35**(1): 117-128.
Ogola, B. O., C. M. Abshire, B. Visniauskas, J. X. Kiley, A. C. Horton, G. L. Clark-Patterson, I. Kilanowski-Doroh, Z. Diaz, A. N. Bicego, A. B. McNally, M. A. Zimmerman, L. Groban, A. J. Trask, K. S. Miller and S. H. Lindsey (2022). "Sex differences in vascular aging and impact of GPER deletion." Am J Physiol Heart Circ Physiol **323**(2): H336-H349.
Omar, N. M., A. M. Abbas, H. Abdel-Malek and G. M. Suddek (2013). "Effect of age on the contractile response of the rat carotid artery in the presence of sympathetic drugs and L-NAME." Acta Physiol Hung **100**(3): 266-279.
Onetti, Y., F. Jiménez-Altayó, M. Heras, E. Vila and A. P. Dantas (2013). "Western-type diet induces senescence, modifies vascular function in non-senescence mice and triggers adaptive mechanisms in senescent ones." Exp Gerontol **48**(12): 1410-1419.
Pettigrew, L. C., N. Thomas, V. J. Howard, R. Veltkamp and J. F. Toole (2000). "Low mini-mental status predicts mortality in asymptomatic carotid arterial stenosis. Asymptomatic Carotid Atherosclerosis Study investigators." Neurology **55**(1): 30-34.

659 Pfaltzgraff, E. R., E. L. Shelton, C. L. Galindo, B. L. Nelms, C. W. Hooper, S. D. Poole,
660 P. A. Labosky, D. M. Bader and J. Reese (2014). "Embryonic domains of the aorta
661 derived from diverse origins exhibit distinct properties that converge into a common
662 phenotype in the adult." J Mol Cell Cardiol **69**: 88-96.
663 Proudman, R. G. W., A. S. Pupo and J. G. Baker (2020). "The affinity and selectivity of
664 α-adrenoceptor antagonists, antidepressants, and antipsychotics for the human α1A,
665 α1B, and α1D-adrenoceptors." Pharmacol Res Perspect **8**(4): e00602.
666 Sakuma I, Liu MY, Sato A, Hayashi T, Iguchi A, Kitabatake A, Hattori Y. (2002).
667 Endothelium-dependent hyperpolarization and relaxation in mesenteric arteries of
668 middle-aged rats: influence of oestrogen. Br J Pharmacol. **135**(1):48-54.
669 Sverdlov, A. L., D. T. Ngo, W. P. Chan, Y. Y. Chirkov and J. D. Horowitz (2014). "Aging
670 of the nitric oxide system: are we as old as our NO?" J Am Heart Assoc **3**(4).
671 Takahashi, T. A. and K. M. Johnson (2015). "Menopause." Med Clin North Am **99**(3):
672 521-534.
673 Tang, E. H. and P. M. Vanhoutte (2008). "Gene expression changes of prostanoid
674 synthases in endothelial cells and prostanoid receptors in vascular smooth muscle
675 cells caused by aging and hypertension." Physiol Genomics **32**(3): 409-418.
676 Wang, A., X. Liu, G. Chen, H. Hao and Y. Wang (2017). "Association between Carotid
677 Plaque and Cognitive Impairment in Chinese Stroke Population: The SOS-Stroke
678 Study." Sci Rep **7**(1): 3066.
679 Willie, C. K., Y. C. Tzeng, J. A. Fisher and P. N. Ainslie (2014). "Integrative regulation
680 of human brain blood flow." J Physiol **592**(5): 841-859.
681 Zhong, W., K. J. Cruickshanks, C. R. Schubert, C. W. Acher, C. M. Carlsson, B. E.
682 Klein, R. Klein and R. J. Chappell (2012). "Carotid atherosclerosis and 10-year
683 changes in cognitive function." Atherosclerosis **224**(2): 506-510.
684

685 **Tables**

686

687 **Table 1.** Basic parameters of 8-months-old SAMR1 and SAMP8 female mice

	SAMR1	SAMP8
Body Weight (g)	25.8± 0.4	30.6±0.7*
Abdominal fat (mg tissue / cm tíbia)	0.19±0.05	0.42±0.03*
Gastrocnemius dry (mg tissue/cm tíbia)	0.029±0.002	0.0016±0.002*
Uterus dry (mg tissue/cm tíbia)	0.023±0.003	0.010±0.001*
Tail cuff blood pressure (mmHg)	113±3	107±7
Estrogen (pg / mL)	9.25±2.5	7.04±1.13
Progesterone (pg / mL)	68.35±45	72.97±86
Testosterone (ng / ml)	6.65±13.3	6.85±4.5

688 Results are expressed as mean ± SEM of 5 animals/group. Statistical significance was
689 calculated by unpaired T-test with Welch's correction. * $p<0.05$ vs. SAMR1

690

Figures Legends

Figure 1 – Senescence induced changes in adrenergic vasocontraction. Cumulative concentration-response curves to phenylephrine (Phe) **(A)**, U46619 **(B)**, acetylcholine (ACh) **(C)**, and sodium nitroprusside (SNP) **(D)** in endothelium-intact common carotid artery from 8-months old SAMR1 and SAMP8 females. Inset graphs are mean ± SEM of the area under the curve calculated from each concentration-response curve (n = 6-11 mice/group). Statistical significance was calculated by the extra sum-of-squares F (fit of concentration-response curves) and T-test with Welch's correction (AUC). P-values and comparisons are expressed on top of Box & Whiskers plots and by the curves. Significance is considered when $p < 0.05$.

Figure 2 – Impact of senescence on endothelium-derived factors and Phe contraction. Cumulative concentration-response curves to phenylephrine (Phe) in endothelium-intact common carotid artery from 8-months old SAMR1 and SAMP8 females. The role of NO, O2- and prostanoids in Phe-induced contraction was assessed by treatment with L-NAME **(A and B)**, tempol **(C and D),** and indomethacin **(E and F).** Inset graphs are mean ± SEM of the area under the curve calculated from each concentration-response curve (n = 6-12 mice/group). **(G)** represent the delta difference in the AUC of basal vs. treated arteries. Statistical significance was calculated by the extra sum-of-squares F (fit of concentration-response curves) and T-test with Welch's correction (AUC). P-values and comparisons are expressed on top of Box & Whiskers plots and by the curves. Significance is considered when $p < 0.05$.

Figure 3 – Impact of senescence on COX-mediated signaling pathway. Cumulative concentration-response curves to phenylephrine (Phe) in endothelium-intact common carotid artery from 8-months old SAMR1 and SAMP8 females. The role of COX-1- and COX-2- derived prostanoids to Phe-induced contraction was assessed by treatment with selective COX-1 **(A and C)** or COX-2 **(B and D)** inhibitors**.** Inset graphs are mean ± SEM of the area under the curve calculated from each concentration-response curve (n = 6-11 mice/group). The levels of prostacyclin **(E),** thromboxane A2 **(F)**, and the ratio of release **(G)** were determined after concentration-response curves to Phe. The expression of mRNA of COX-1 **(H)** and COX-2 **(I)** was determined in the common carotid of SAMR1 and SAMP8. Statistical significance was calculated by the extra sum-of-squares F (fit of concentration-response curves) and T-test with Welch's correction (AUC). P-values and comparisons are expressed on top of Box & Whiskers plots and by the curves. Significance is considered when $p < 0.05$.

Figure 4 – Role of senescence on α1-adrenergic receptor-mediated contraction. Cumulative concentration-response curves to phenylephrine (Phe) in endothelium-intact common carotid artery from 8-months old SAMR1 and SAMP8 females. The contribution of specific alpha-adrenergic receptors to Phe-induced contraction was determined by pre-treatment of arteries with α-$_{1A}$ adrenergic antagonist (5 methyl-urapidil, n =8) and α-$_{1D}$ adrenergic antagonist (BMY 7378, n=8). The antagonist concentrations of 5 methyl-urapidil **(A)** and BMY 7378 **(B)** to be used in the studies concertation were tested in the common carotid of SAMR1 and then tested as a single concentration (10^{-7}M) in the common carotid of SAMR1 **(C and D)** and SAMP8 **(E and F).** The density of α1-adrenergic receptors was determined in the primary culture of VSMC from SAMR1 and SAMP8 **(G)** and normalized by the amount of protein **(H)**. Statistical significance was calculated by the extra sum-of-squares F (fit of concentration-response curves) and T-test with Welch's correction (receptor density and EC50). P-values and comparisons are expressed on top of Box & Whiskers plots and by the curves. Significance is considered when $p < 0.05$.

Figure 5 - Senescence increases intracellular free calcium via the α_{1A}-adrenergic receptor. Schematic representation of protocol for determining intracellular free calcium (iCa^{+2}) in response to Phe (10^{-7} M) in VSMCs of SAMR1 and SAMP8 female mice **(A)**. Time-course of iCa^{+2} in response to Phe stimuli (10^{-7} M) in VSMC of SAMR1 and SAMP8, and in response to Ionomycin, as a positive control **(B)**. Time-course of iCa^{+2} in the absence and the presence of α_{1A} antibody in VSMC of SMAR1 **(C)** and SAMP8 **(D)**. **(E)** Box & Whiskers plots show the differences in the AUC of iCa^{+2} time-course in all groups (n=4 individual sample/group). Statistical significance was calculated by Brown Forsythe and Welch ANOVA, followed by Dunnett's T3 post hoc analysis. P-values and comparisons are expressed on top of Box & Whiskers plots. Significance is considered when $p < 0.05$.

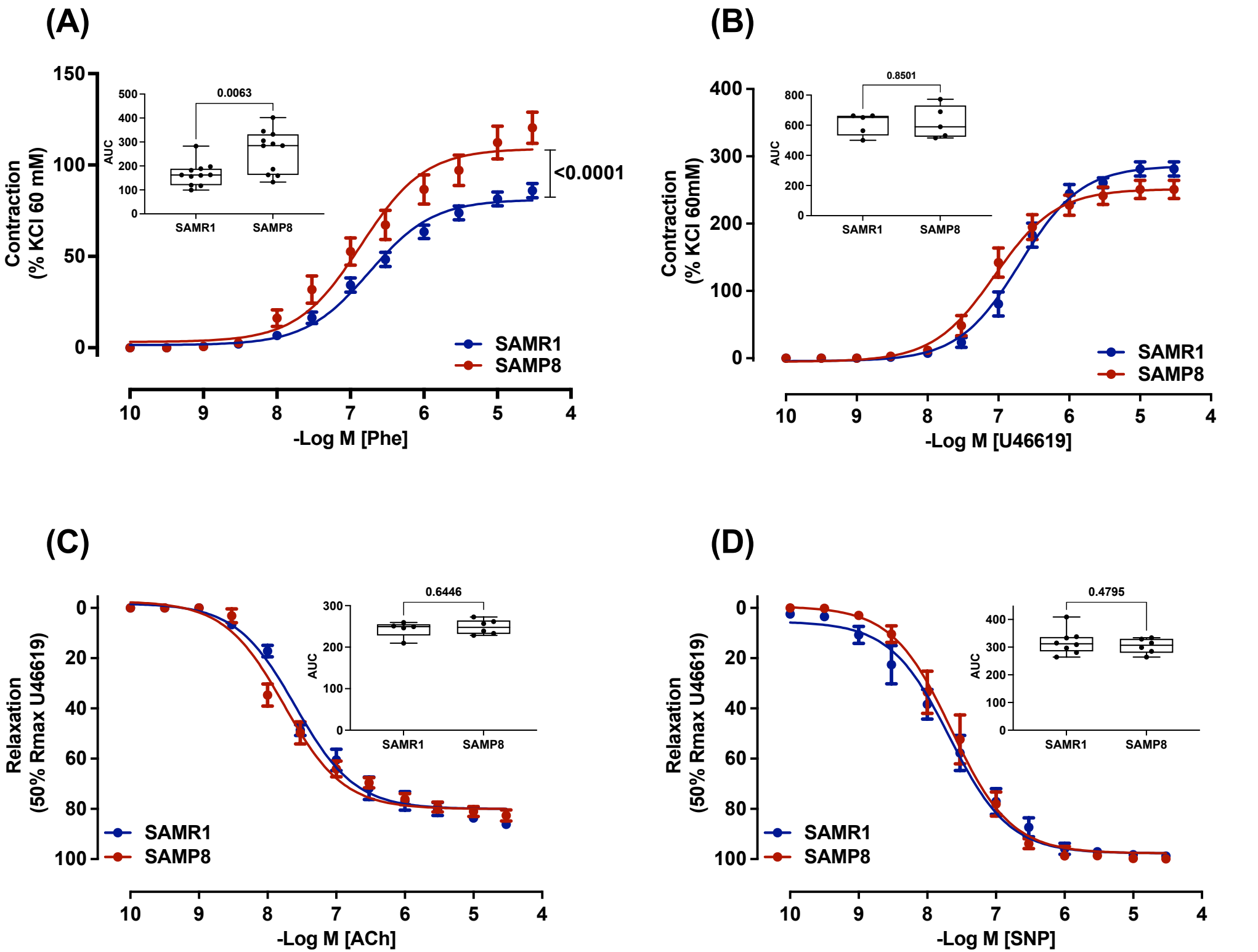
(A)
Contraction (% KCl 60 mM)
150
100
50
0
AUC
500
400
300
200
100
0
0.0063
SAMR1
SAMP8
<0.0001
SAMR1
SAMP8
10
9
8
7
6
5
4
-Log M [Phe]
(B)
Contraction (% KCl 60mM)
400
300
200
100
0
AUC
800
600
400
200
0
0.8501
SAMR1
SAMP8
SAMR1
SAMP8
10
9
8
7
6
5
4
-Log M [U46619]
(C)
Relaxation (50% Rmax U46619)
0
20
40
60
80
100
AUC
300
200
100
0
0.6446
SAMR1
SAMP8
SAMR1
SAMP8
10
9
8
7
6
5
4
-Log M [ACh]
(D)
Relaxation (50% Rmax U46619)
0
20
40
60
80
100
AUC
400
300
200
100
0
0.4795
SAMR1
SAMP8
SAMR1
SAMP8
10
9
8
7
6
5
4
-Log M [SNP]

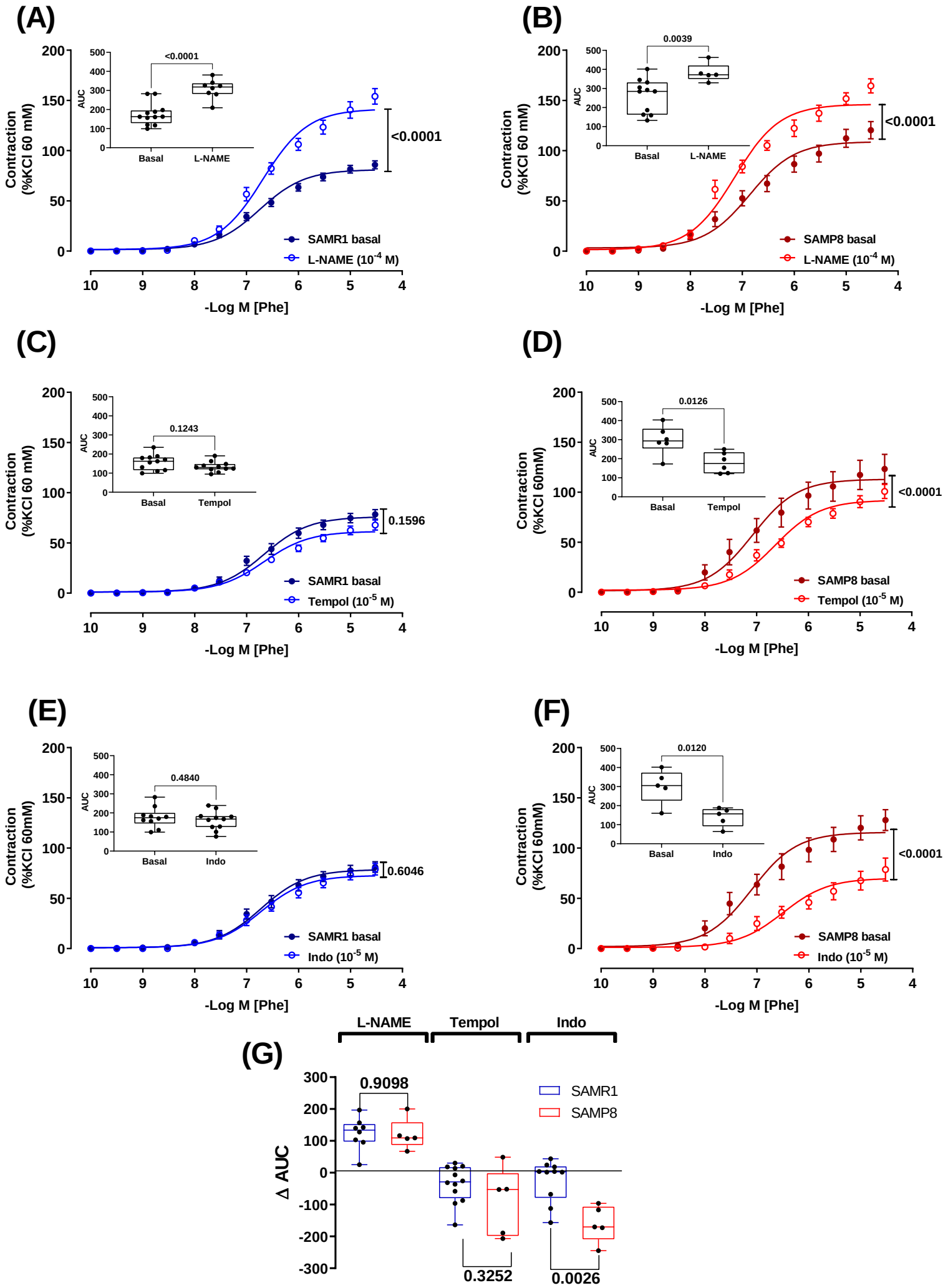
(A)
Contraction (%KCl 60 mM)
AUC
<0.0001
Basal
L-NAME
<0.0001
SAMR1 basal
L-NAME (10-4 M)
-Log M [Phe]
(B)
0.0039
<0.0001
SAMP8 basal
L-NAME (10-4 M)
(C)
0.1243
Tempol
0.1596
SAMR1 basal
Tempol (10-5 M)
(D)
0.0126
<0.0001
SAMP8 basal
Tempol (10-5 M)
(E)
0.4840
Indo
0.6046
SAMR1 basal
Indo (10-5 M)
(F)
0.0120
<0.0001
SAMP8 basal
Indo (10-5 M)
(G)
L-NAME
Tempol
Indo
Δ AUC
0.9098
SAMR1
SAMP8
0.3252
0.0026

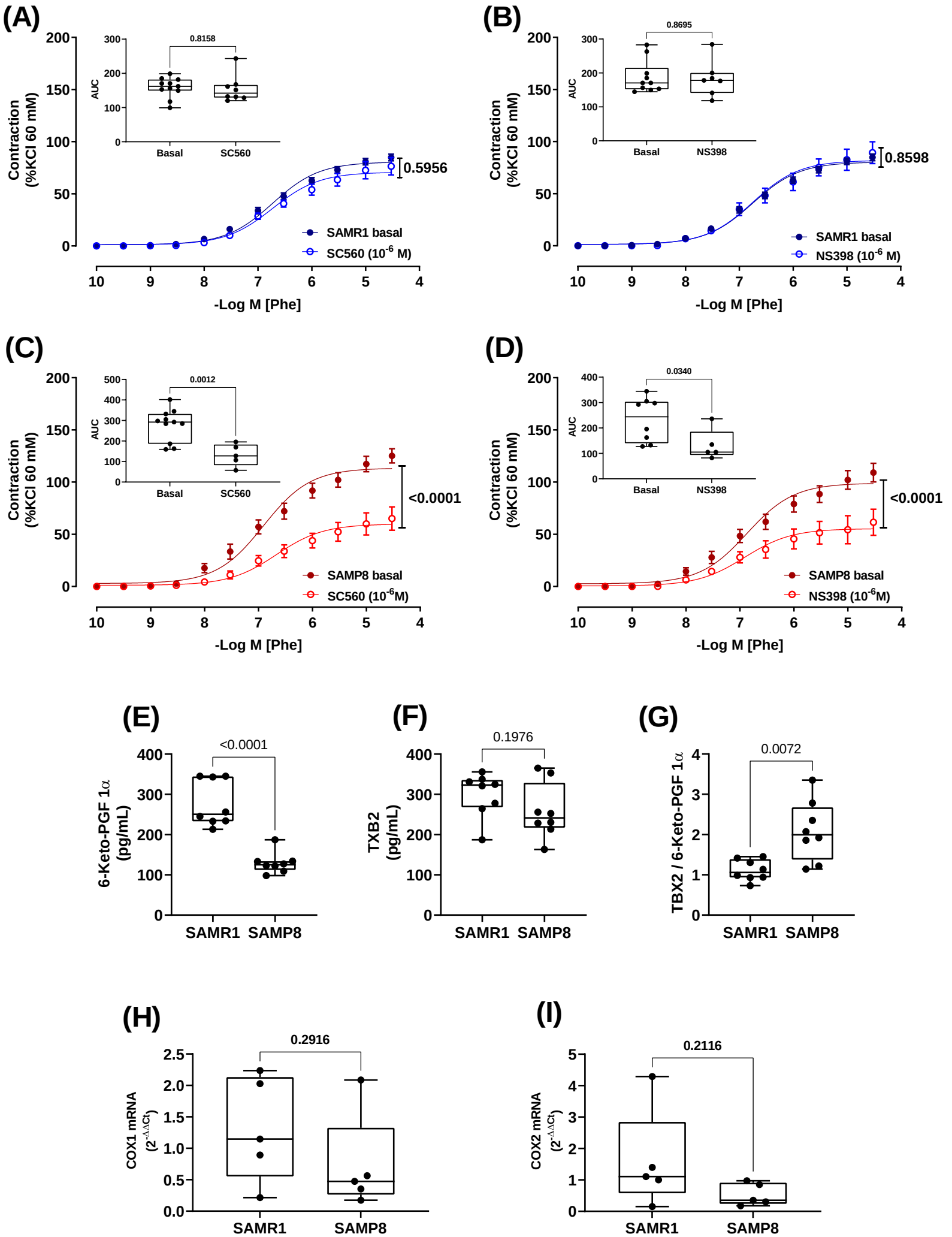
(A)
Contraction (%KCl 60 mM)
AUC
0.8158
Basal
SC560
0.5956
SAMR1 basal
SC560 (10-6 M)
-Log M [Phe]
(B)
0.8695
NS398
0.8598
NS398 (10-6 M)
(C)
0.0012
<0.0001
SAMP8 basal
SC560 (10-6M)
(D)
0.0340
NS398 (10-6M)
(E)
6-Keto-PGF 1α (pg/mL)
<0.0001
SAMR1 SAMP8
(F)
TXB2 (pg/mL)
0.1976
(G)
TBX2 / 6-Keto-PGF 1α
0.0072
(H)
COX1 mRNA (2-ΔΔCt)
0.2916
(I)
COX2 mRNA (2-ΔΔCt)
0.2116

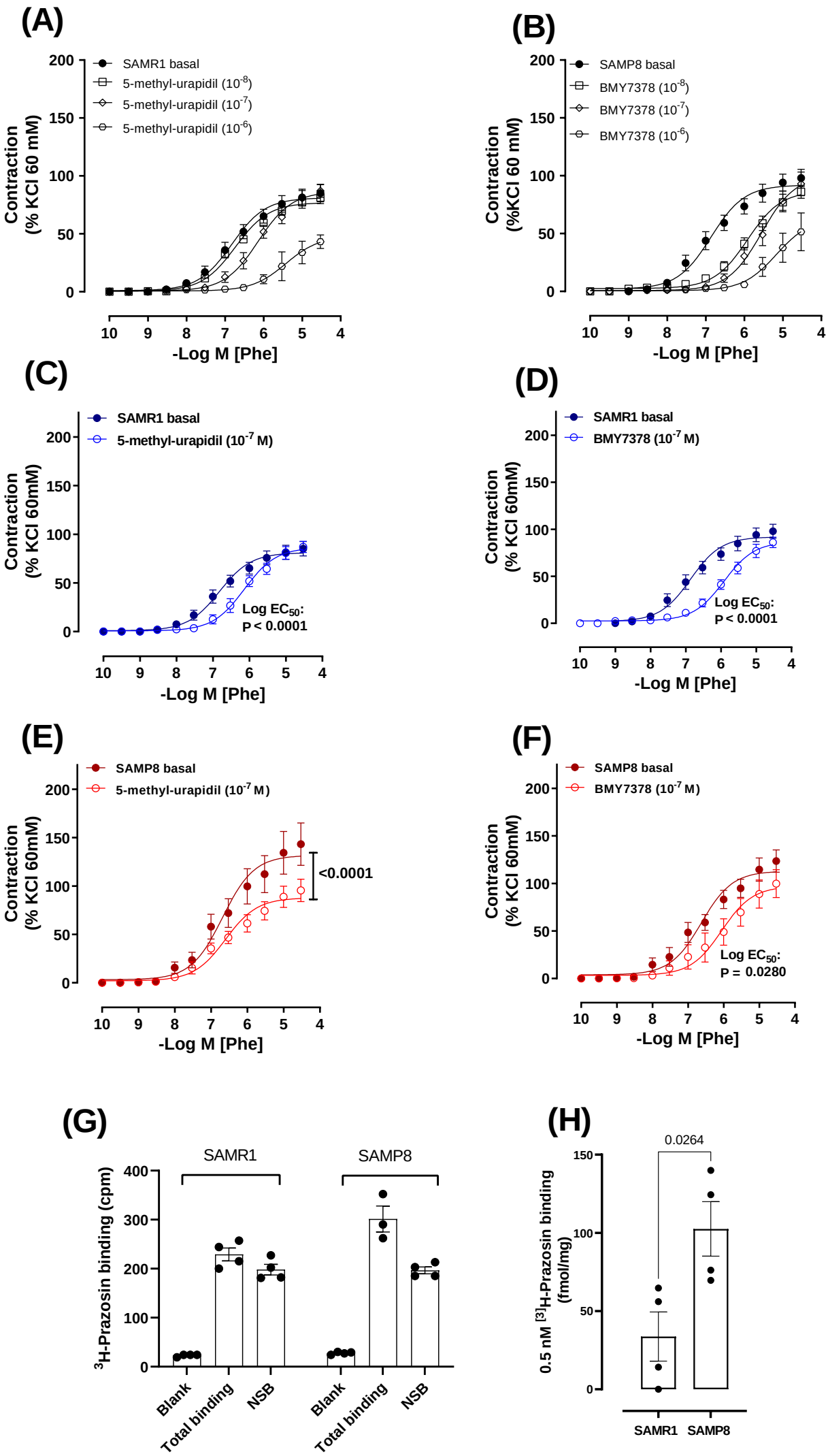
(A)
SAMR1 basal
5-methyl-urapidil (10-8)
5-methyl-urapidil (10-7)
5-methyl-urapidil (10-6)
Contraction (% KCl 60 mM)
-Log M [Phe]
(B)
SAMP8 basal
BMY7378 (10-8)
BMY7378 (10-7)
BMY7378 (10-6)
Contraction (%KCl 60 mM)
-Log M [Phe]
(C)
SAMR1 basal
5-methyl-urapidil (10-7 M)
Contraction (% KCl 60mM)
Log EC50:
P < 0.0001
-Log M [Phe]
(D)
SAMR1 basal
BMY7378 (10-7 M)
Contraction (% KCl 60mM)
Log EC50:
P < 0.0001
-Log M [Phe]
(E)
SAMP8 basal
5-methyl-urapidil (10-7 M)
Contraction (% KCl 60mM)
<0.0001
-Log M [Phe]
(F)
SAMP8 basal
BMY7378 (10-7 M)
Contraction (% KCl 60mM)
Log EC50:
P = 0.0280
-Log M [Phe]
(G)
SAMR1
SAMP8
3H-Prazosin binding (cpm)
Blank
Total binding
NSB
Blank
Total binding
NSB
(H)
0.0264
0.5 nM [3]H-Prazosin binding (fmol/mg)
SAMR1
SAMP8

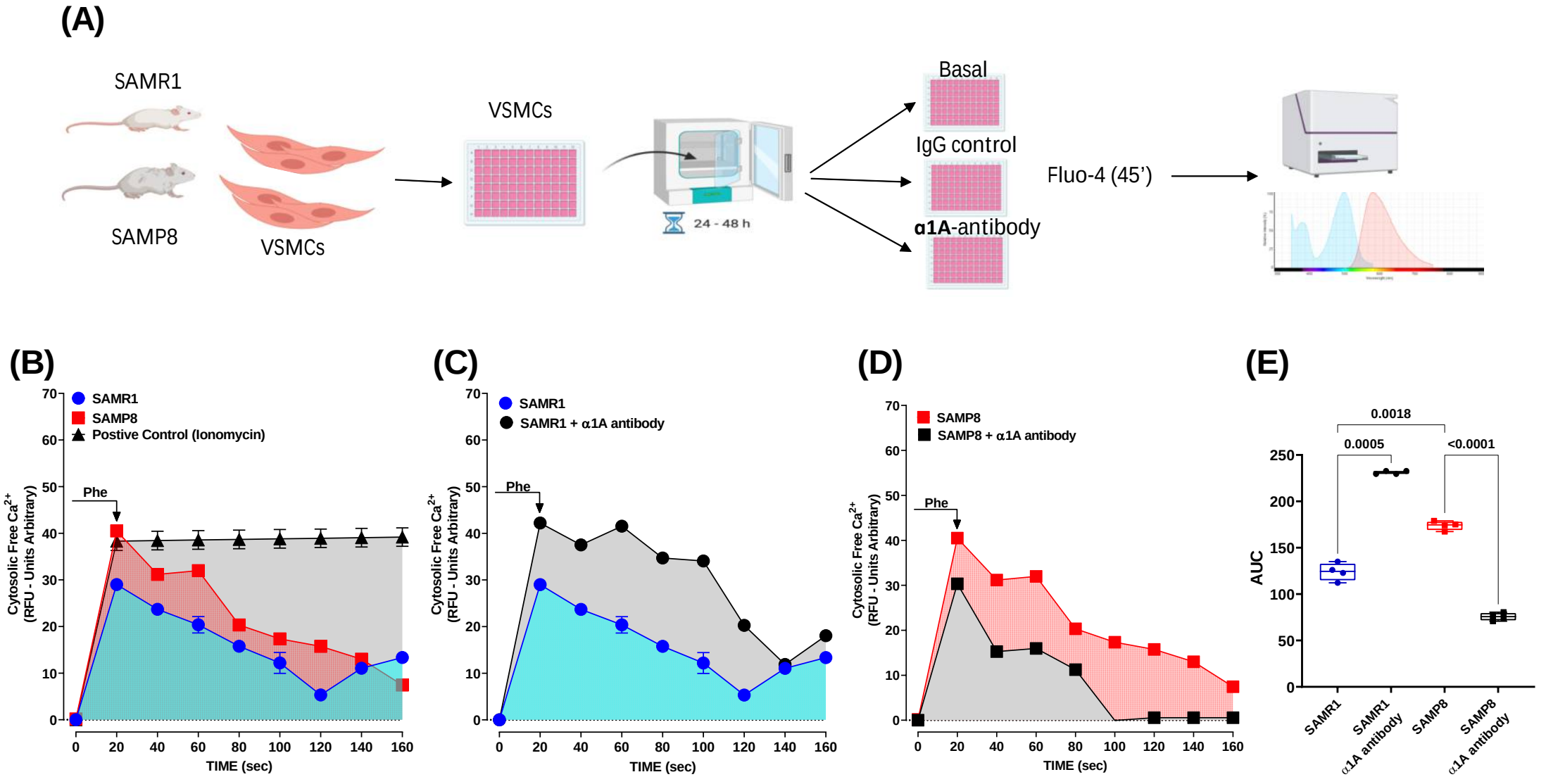
(A)
SAMR1
SAMP8
VSMCs
VSMCs
24 - 48 h
Basal
IgG control
α1A-antibody
Fluo-4 (45')
(B)
SAMR1
SAMP8
Postive Control (Ionomycin)
Phe
Cytosolic Free Ca2+ (RFU - Units Arbitrary)
TIME (sec)
(C)
SAMR1
SAMR1 + α1A antibody
Phe
Cytosolic Free Ca2+ (RFU - Units Arbitrary)
TIME (sec)
(D)
SAMP8
SAMP8 + α1A antibody
Phe
Cytosolic Free Ca2+ (RFU - Units Arbitrary)
TIME (sec)
(E)
0.0018
0.0005
<0.0001
AUC
SAMR1
SAMR1 α1A antibody
SAMP8
SAMP8 α1A antibody

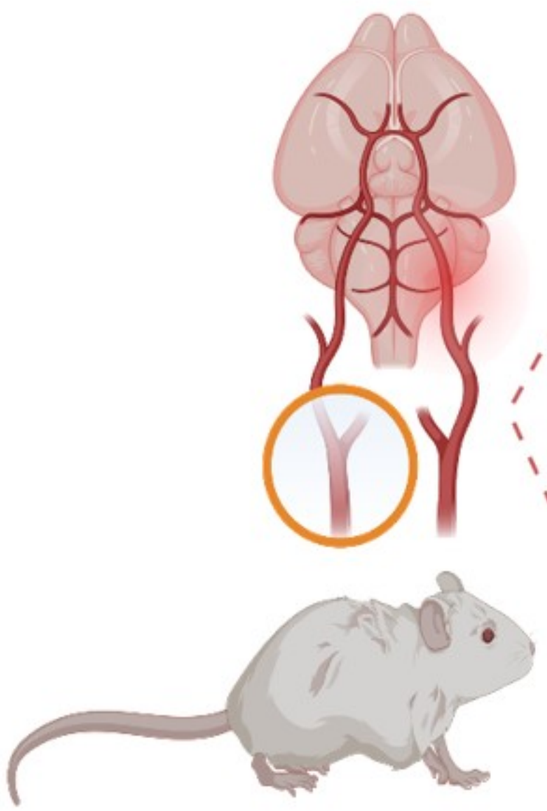

Senescence-accelerated
female mice

α1 A adrenergic receptor

Ca^{2+}

COX-1

PGI_2

PE-induced
vasoconstriction

Carotid dysfuction

SUPPLEMENTARY MATERIAL

Carotid dysfunction in senescent female mice is mediated by increased α_{1A}-adrenoceptor activity and COX-derived vasoconstrictor prostanoids.

Running title: vascular α-adrenergic dysfunction in female senescent mice

Tiago J. Costa[a,d], Paula R. Barros[a], Diego A. Duarte[a,b], Júlio A. Silva-Neto[a], Sara Cristina Hott[a], Thamyris S. Silva[a], Claudio M. Costa-Neto[b], Felipe V. Gomes[a], Eliana H. Akamine[c], Cameron G McCarthy[d], Francesc Jimenez-Altayó[e], Ana Paula Dantas*[f]. Rita C. Tostes*[a]

[a] Department of Pharmacology, Ribeirao Preto Medical School, University of São Paulo, Ribeirão Preto, SP, Brazil.
[b] Department of Biochemistry and Immunology, School of Medicine. campus Ribeirão Preto, University of São Paulo, Ribeirão Preto, SP, Brazil.
[c] Department of Pharmacology, Institute of Biomedical Sciences, University of São Paulo, São Paulo, SP, Brazil.
[d] Cardiovascular Translational Research Center, Department of Cell Biology and Anatomy, University of South Carolina, Columbia, South Carolina.
[e] Department of Pharmacology, Therapeutic. and Toxicology, School of Medicine, Neuroscience Institut, Universitat Autònoma de Barcelona, Bellaterra, Spain.
[f] Laboratory of Experimental Cardiology, Institut d'Investigacions Biomediques August Pi i Sunyer (IDIBAPS), Hospital Clinic Cardiovascular Institute, Barcelona, Spain.

*Equal contribution

Corresponding Author:
Ana Paula Dantas - Laboratory of Experimental Cardiology, August Pi i Sunyer Biomedical Research Institute (IDIBAPS), Hospital Clinic Cardiovascular Institute, Barcelona, Spain.
adantas@recerca.clinic.cat

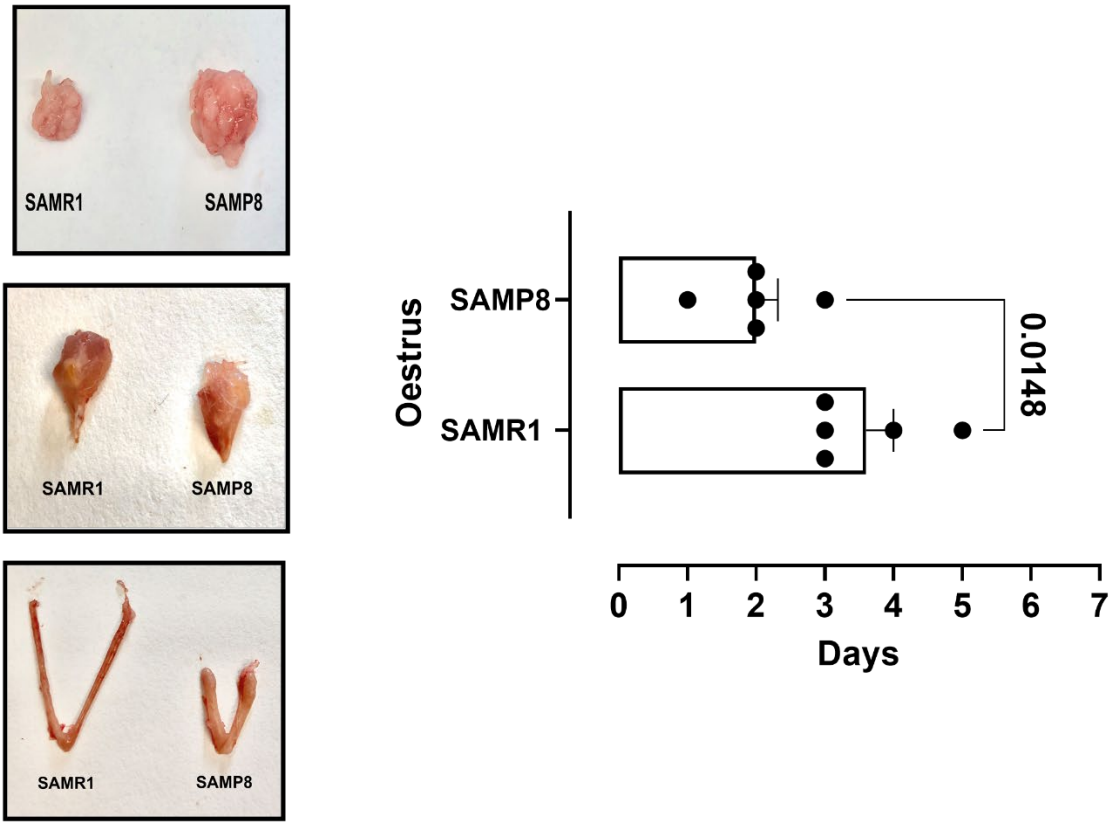

Figure S1 - Representative image of adipose tissue, gastrocnemius, and uterus from SAMR and SAMP8 mice at 8 months old. Duration of estrus cycle (days) in SAMR1 (n=5) and SAMP8 (n=5) female mice. The estrous cycle phase was determined daily by vaginal smears during a 7- day period. Statistical significance was calculated by unpaired T-test with Welch's correction. p-values and comparisons are expressed on top of bar graphs. Significance is considered when $p < 0.05$.

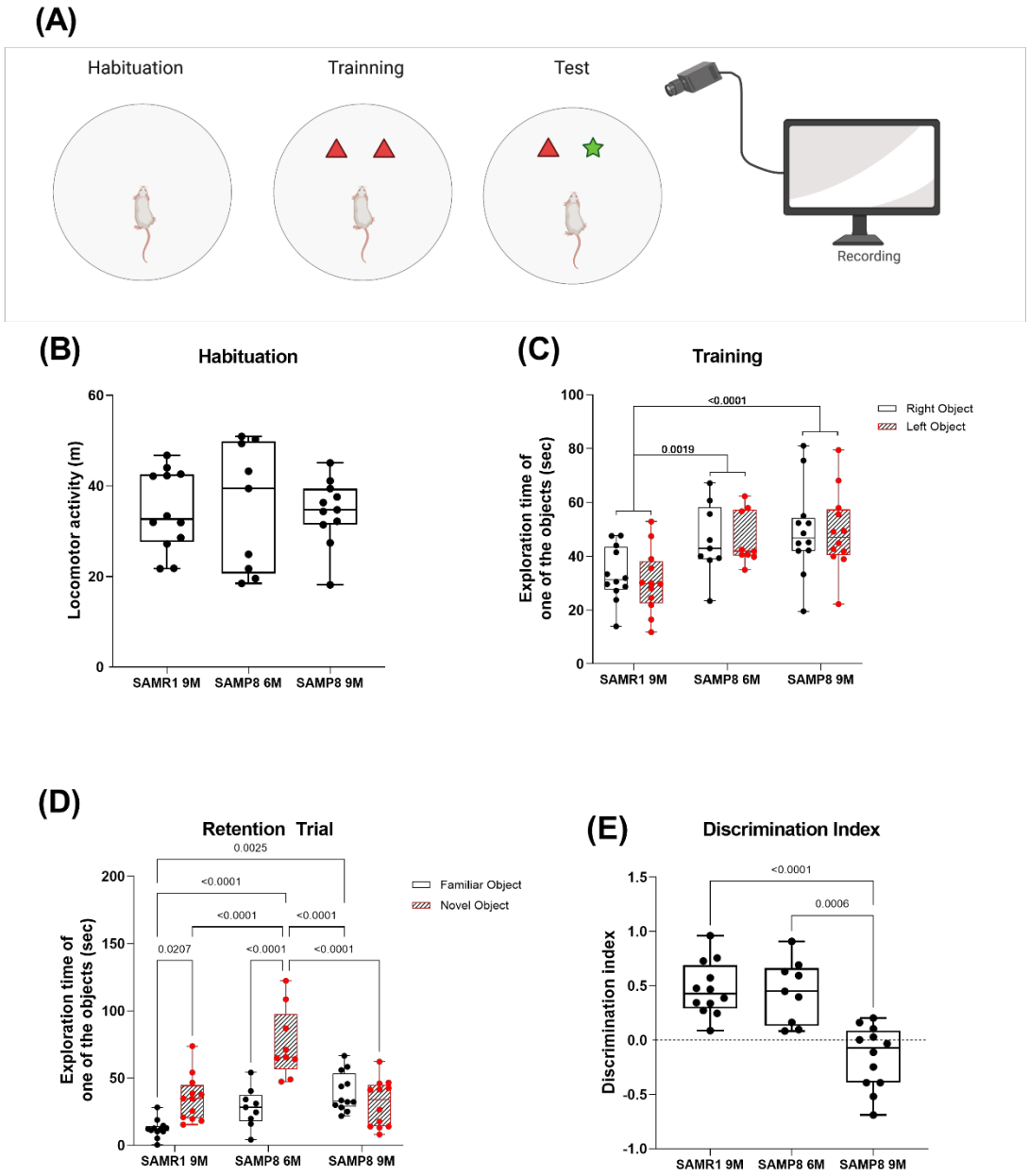

Figure S2 – Cognitive function in SAMP8. A discrimination index design indicates cognitive dysfunction in females SAMR1 and SAMP8 **(A).** The discrimination index was determined in 9-month SAMR1 (SAMR1 9M, n=12), 6-month SAMP8 (SAMP8 6M, n=9), and 8-month SAMP8 (SAMP8 9M, n=12). After habituation **(B)** and training **(C)** sessions, cognition capacity was determined by the time spent in a familiar object vs a novel object **(D)** and calculated as discrimination index **(E)**. Box & Whiskers plots represent the mean ± SEM from independent experiments. Statistical significance was calculated by Brown Forsythe and Welch ANOVA, followed by Dunnett's T3 post hoc analysis. P-values and comparisons are expressed on top of Box & Whiskers plots. Significance is considered when $p < 0.05$.

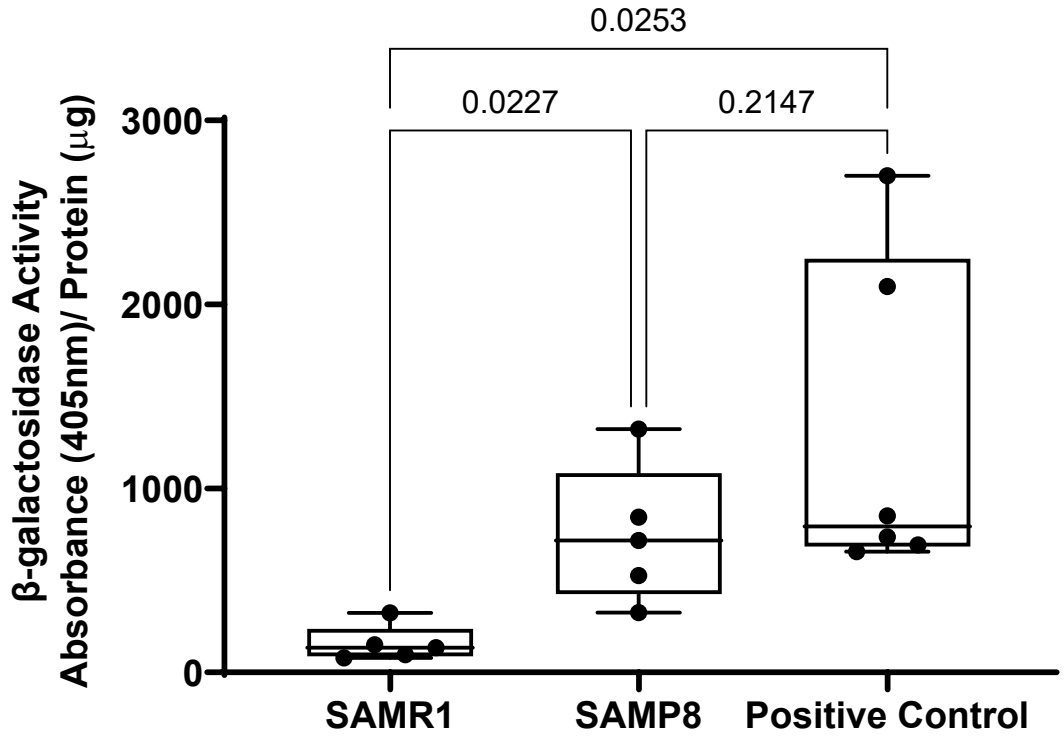

Figure S3 - Values of relative absorbance of β-galactosidade activity normalized by the amount of protein. Liver from C57/Blc6 with 12 months was used as a positive control. Box & Whiskers plots represent the variation (median + interquartile range) of independent set of data (n=5/group). Statistical significance was calculated by Brown Forsythe and Welch ANOVA, followed by Dunnett's T3 post hoc analysis. p-values and comparisons are expressed on top of bar graphs. Significance is considered when $p < 0.05$.

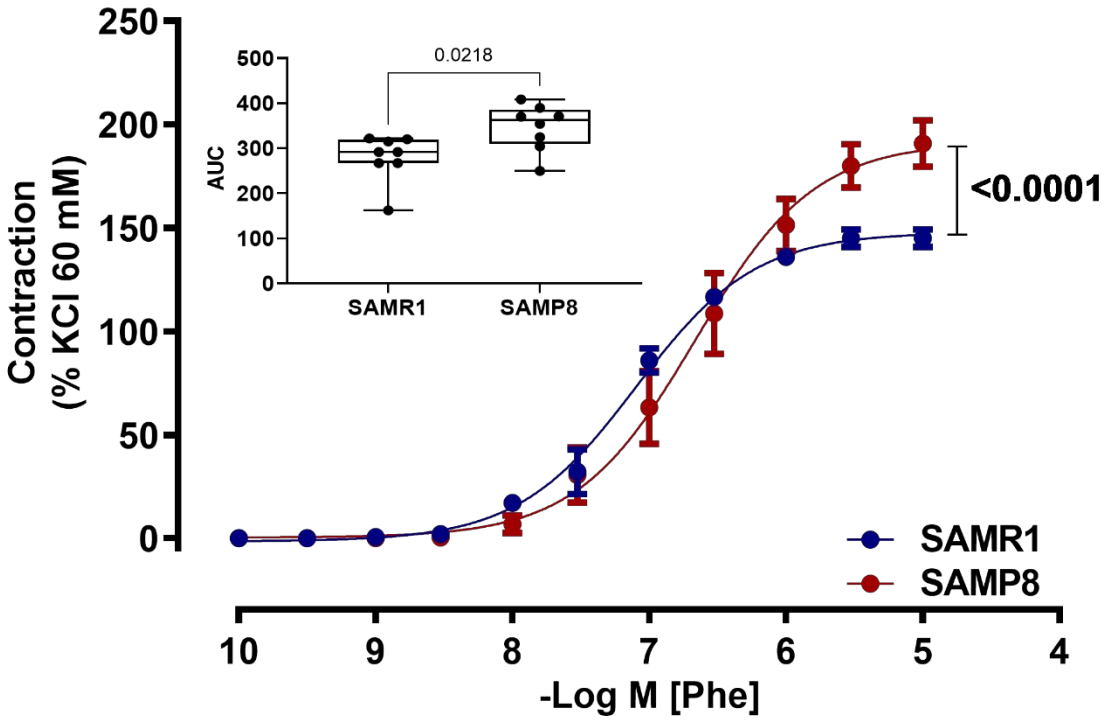

Figure S4 – **Senescence-induced changes in adrenergic vasocontraction in carotid arteries without endothelium**. Cumulative concentration-response curves to phenylephrine (Phe) in endothelium-denuded common carotid artery from 8-months old SAMR1 (n=8) and SAMP8 (n=8) females. Inset box plots are the variation (median + interquartile range) of the area under the curve calculated from each concentration-response curve. Statistical significance was calculated by the extra sum-of-squares F (fit of concentration-response curves) and T-test with Welch's correction (AUC). P-values and comparisons are expressed on top of bar graphs and by the curves. Significance is considered when $p < 0.05$.

Supplementary Table S1 – Potency (pD_2) and maximal effect (Emax) to Phenylephrine in carotid rings with (E+) and without (E-) endothelium from SAMR1 and SAMP8 mice.

	Mean + (95% CI)		
	SAMR1	**SAMP8**	p Value
pD_2 E+	6.7 (6.38 – 7.02)	6.8 (6.54 – 7.12)	0.5079
pD_2 E-	7.1 (6.87 – 7.32)	6.7 (6.24 – 7.24)	0.1586
Emax E+	81.1 (77.7 – 84.6)	108.9 (101.5 -116.3)	0.0001
Emax E-	147.2 (142.6 -151.8)	191.8 (179.1 – 204.5)	0.0001

Values are mean with 95% CI. Significance is considered when $p < 0.05$.